Theoretical Study of Stable, Defect-Free $(TiO_2)_n$ Nanoparticles with n = 10–16

ARTICLE *in* THE JOURNAL OF PHYSICAL CHEMISTRY C · OCTOBER 2007

Impact Factor: 4.77 · DOI: 10.1021/jp073988t

Theoretical Study of Stable, Defect-Free $(TiO_2)_n$ Nanoparticles with $n = 10-16$

Zheng-wang Qu* and Geert-Jan Kroes

Leiden Institute of Chemistry, Gorlaeus Laboratories, Leiden University, P.O. Box 9502, 2300 RA Leiden, The Netherlands

Received: May 23, 2007; In Final Form: August 6, 2007

Novel defect-free $(TiO_2)_n$ nanoparticles can be very useful for mechanistic studies of photooxidation of water and organic pollutants on nanostructured oxide materials involving surface-trapped electrons and holes. In this study, the electronic structure and stability of $(TiO_2)_n$ nanoparticles with $n = 10-16$ (~1 nm in diameter) have been investigated using the density functional B3LYP/LANL2DZ method to find stable, Ti═O defect-free structures. The even-n $(TiO_2)_n$ clusters tend to form compact (rather than linear or cyclic) covalent networks consisting of only 4-coordinated $Ti^{(4)}$ and 2-coordinated $O^{(2)}$ atoms, while odd-n clusters tend to form more ionic structures with additional highly coordinated Ti and O atoms. The new half-spherical $(TiO_2)_{15}$ **15b** cluster represents the smallest defect-free rutile nanocrystal. Strong vibrational bands around 770 and 820 cm^{-1} are found to be useful for identifying surface $O^{(2)}$ and $O^{(3)}$ species, respectively. Consistent with the odd−even oscillation of structural features of stable $(TiO_2)_n$ nanoparticles, various electronic properties, including cluster formation energies, HOMO−LUMO gaps, vertical excitation energies, and ionization potentials, also show odd−even oscillations. Strong interatomic O(2p) lone pair interactions that destabilize the highest occupied molecular orbitals of the $(TiO_2)_n$ clusters can significantly reduce the lowest vertical excitation energy to values significantly below the band gap of bulk TiO_2 for clusters with odd n. If materials can be engineered to incorporate such $(TiO_2)_n$ nanoparticles, they could exhibit visible light photoactivity. The electron holes are shown to be localized mainly on surface $O^{(1)}$ and $O^{(2)}$ rather than $O^{(3)}$ sites, suggesting that a recently proposed water photooxidation mechanism [Nakamura et al. *J. Am. Chem. Soc.* **2005**, *127*, 12975] should be revised.

1. Introduction

Nanostructured TiO_2 materials are widely used for various applications,[1−10] for instance, as photocatalysts for sustainable hydrogen production from solar energy and water,[1−3] for photochemical removal of organic pollutants in water and in air,[4−6] or simply as stable white UV-proof pigments. Advantages of TiO_2 are that it is inexpensive and chemically and biologically inert.[6,7] The TiO_2 semiconductor catalyst has a large band gap (3−3.2 eV)[11] and is very stable under illumination for water photolysis, but it absorbs only the ultraviolet part of the solar emission, thus limiting its efficiency for solar energy conversion. There are extensive recent efforts to extend the visible light activity of TiO_2, mainly by dye-sensitizing and incorporating the photoelectrolysis cell into a tandem cell[1] and by doping with different anions (N, S, C) that replace oxygen in the crystal lattice.[12−19] Recently, even nanotube and amorphous TiO_2 specimens are found to exhibit some visible light activity in photocatalytic reactions,[20,21] possibly due to structural defects such as oxygen vacancies[21] and/or to the existence of surface states of trapped electrons[22] and holes.[23,24]

In nature, TiO_2 exists as mainly rutile and anatase crystals, with the former being about 2.6 kJ/mol more stable under ambient conditions.[25,26] However, the anatase phase is found to be more stable than the rutile phase when the particle diameters of TiO_2 are in the range of 2−14 nm.[27] For even smaller nanoparticles, only a few charged[28] and neutral[29] clusters have been produced experimentally, without information on their structure. In general, new nanostructures could be expected when the particle diameter becomes smaller than some crossover point. We are particularly interested in small TiO_2 nanoparticles of about 1 nm for several reasons. First, the stable structures of small TiO_2 particles themselves are of interest from a fundamental point of view. Second, given the cosmic abundances of the elements Ti and O, small $(TiO_2)_n$ clusters are also of astrophysical interest, due to their possible role in dust formation processes in circum-stellar shells of oxygen-rich stars.[29] Third, it might be possible to find clusters with enhanced visible light activity (small band gap). Finally, small TiO_2 nanoparticles can be employed in the detailed study of photooxidation of water on TiO_2 surfaces or, more generally, photochemistry on TiO_2 surfaces. Recent experimental data have suggested that the photoevolution of oxygen on TiO_2 surfaces should be initiated by the nucleophilic attack of a H_2O molecule on a surface-trapped hole.[24] Efficient catalysts, particularly for the four-electron process of oxygen generation, have however not yet been found. A detailed mechanical study could be helpful in improving the efficiency and stability of photocatalysts for water oxidation.

Generally, electron−hole pairs are created within semiconductor electrodes after the above band gap photon absorption and then diffuse to the surface to perform oxidation (by holes) or reduction (by electrons) reactions. To get some insight into the molecular reaction steps of water splitting and, more specifically, the oxidation of water on semiconductor oxide surfaces, we have recently performed[30] (contributed to[31]) periodic DFT studies of some crucial intermediate structures such as coadsorbed H_2O and O, OH, and OOH species on the

* To whom correspondence should be addressed. E-mail: z.qu@chem.leidenuniv.nl.

10.1021/jp073988t CCC: $37.00
Published on Web 10/16/2007

most stable rutile-type (110) oxide surfaces of TiO_2, RuO_2 and IrO_2. However, further understanding the nature of the reactions of H_2O and reaction intermediates with surface-trapped holes on both bare and hydrated surfaces is still desirable,[32−36] for which reasonable theoretical nanocluster models are potentially more useful than normal slab models for crystal surfaces.

Basically, two theoretical ways to construct atomistic structures of TiO_2 nanoclusters are found in the literature: either a brute force search is performed for the most stable structure(s)[37,38] or clusters are carved from bulk crystals.[39−41] Global minima of small $(TiO_2)_n$ clusters with $n = 1-15$ have been proposed using a pair-potential model, followed by density functional theory (DFT) calculations to refine the final TiO_2 structures and energies.[37] Recently, we have presented a very detailed DFT study on the stability and electronic structures of neutral and/or charged $(TiO_2)_n$ clusters with $n = 1-9$ and have found new global minima for most cases, with terminal Ti═O groups as a common structural feature on which the photon-created holes tend to be localized.[38] This study suggested that the applicability of the pair-potential model[37] to predict structures of semicovalent $(TiO_2)_n$ nanoparticles is somewhat questionable. Very recently, some anatase TiO_2 nanocrystals have also been constructed with sizes of ≤ 2 nm and studied using DFT calculations,[39] based on some general bonding principles such as nonpolarity and high coordination number,[40] and with sizes of ≤ 6 nm using the self-consistent tight-binding method and Wulff construction.[41] However, a common feature of the optimized nanoparticle structures is that they have at least two defective Ti═O groups at their surface.[39,41] Because this may represent an artifact and because holes tend to localize at Ti═O defects, the use of these clusters for studies of the photoactivity of TiO_2 may be limited.

In this work, we extend our previous study to larger $(TiO_2)_n$ clusters with $n = 10-16$, which have diameters of about 1 nm, with special efforts to identify stable structures without terminal Ti═O defects. Our detailed study provides benchmarks which can be used to further examine the applicability of pair-potential models[37] as well as for instance the general bonding principles[40] for predicting TiO_2 nanoparticle structures. Furthermore, we find an interesting odd−even oscillation in the structural features and electronic properties of stable Ti═O defect-free TiO_2 nanoparticles. Our finding that small clusters with odd n may exhibit vertical excitation energies smaller than the band gap of bulk TiO_2 may suggest new ways of synthesizing nanostructured materials incorporating TiO_2 exhibiting visible light photoactivity. Finally, our finding that upon photoexcitation holes tend to localize near bridging surface $O^{(2)}$ atoms rather than 3-fold-coordinated O atoms suggests that a recently proposed mechanism for photooxidation of water[24] on TiO_2 should be revised.

The paper is organized as follows: In section 2 the computational methods used in this work are described. In section 3 the results are presented and discussed. The low-lying structures of neutral singlet $(TiO_2)_n$ nanoparticles are discussed in section 3.1. The infrared spectra and important electronic properties of stable $(TiO_2)_n$ structures are discussed in sections 3.2 and 3.3, respectively. To understand the nature of trapped holes within stable $(TiO_2)_n$ nanoparticles, stable positively charged $(TiO_2)_n^+$ clusters are discussed in section 3.4. Finally, the implications of our theoretical results for photooxidation of H_2O and photochemistry on TiO_2 are discussed in section 3.5. In section 4 the main conclusions are summarized.

2. Computational Methods

All DFT calculations are done using the GAUSSIAN 03 program.[42,43] Becke's three-parameter exchange functional[44] along with Lee−Yang−Parr's correlation functional,[45] i.e., the B3LYP functional, and the standard LANL2DZ basis set[46−49] are chosen in all our calculations. The LANL2DZ basis set involves the D95 basis set on oxygen[46] and the Los Alamos effective core potential plus double-ζ basis set[47−49] on titanium, respectively, leading to 40 basis functions with 103 primitive Gaussians per TiO_2 unit in our calculations. All singlet neutral $(TiO_2)_n$ clusters with $n = 10-16$ are fully optimized and characterized by subsequent harmonic vibrational frequency analysis. The optimized stationary points are verified as real local minima (without any imaginary frequencies), transition states (with only one imaginary frequency), or high-order saddle points (with more than one imaginary frequency). The zero-point energy (ZPE) corrections to the total energies are obtained from the calculated vibrational frequencies.

The reliability of the B3LYP/LANL2DZ method for various properties of small $(TiO_2)_n$ clusters such as optimized geometries, vibrational frequencies, cluster formation energies, ionization potentials, and singlet−triplet gaps has been tested in our recent study, with the deviations being within 0.01 Å for bond lengths and 0.1 eV for energies from (limited) available experimental data.[38] Such good agreement gives us strong confidence in further applying the B3LYP/LANL2DZ method to larger $(TiO_2)_n$ nanoparticles in this work.

To identify the stable structures of $(TiO_2)_n$ particles, about 10 initial structures for each n value are fully optimized and tested, with special effort to avoid terminal Ti═O structural defects. Stable TiO_2 nanoparticles without defects such as terminal Ti═O could be useful for further mechanistic study of water photooxidation on TiO_2 surfaces. The initial structures are constructed mainly on the basis of information about smaller stable clusters of refs 37 and 38 and by carving out clusters from bulk TiO_2 anatase and rutile structures. We only consider the singlet neutral clusters since the corresponding triplet states have been found to be about 1.4−2.5 eV less stable.[38] For each n value of the $(TiO_2)_n$ cluster, the relative energies (eV) of different structures are obtained by taking the ZPE-corrected total energy of the most stable singlet neutral structure as energy zero. To compare the stability of $(TiO_2)_n$ particles with different n values, we define the cluster formation energy per TiO_2 unit (E_{CF}) as follows:

$$E_{CF}[(TiO_2)_n] = E[(TiO_2)_n]/n - E[TiO_2] \quad (1)$$

where $E[(TiO_2)_n]$ and $E[TiO_2]$ are the total energies including ZPE corrections of the $(TiO_2)_n$ cluster and the free TiO_2 molecule, respectively. Of course, since there are a very large number of possible structures for each $(TiO_2)_n$ with $n = 10-16$, it is possible that a more stable structure than the ones presented here can be found. The low-lying structures presented in this work may serve as *useful TiO_2 nanoparticle models*, but they do not necessarily represent the true global minima.

For some stable $(TiO_2)_n$ structures, time-dependent[50−52] B3LYP/LANL2DZ (TDDFT/B3LYP) calculations are performed to provide vertical excitation energies to the lowest singlet and triplet excited states. Such excitation energies can be compared directly with experimentally observable optical absorption bands and/or the band gaps of TiO_2 nanoparticles and bulk TiO_2. The vertical ionization potentials (IP_V) are calculated by single-point B3LYP/LANL2DZ calculations at optimized neutral cluster geometries for singly positively charged clusters, i.e., a cluster with an electron hole on it:

$$IP_V = E[(TiO_2)_n^+] - E[(TiO_2)_n] \quad (2)$$

Here $E[(TiO_2)_n^+]$ and $E[(TiO_2)_n]$ are the total energies of charged and neutral clusters, respectively, without ZPE correction to the charged clusters and the neutral clusters. Furthermore, the adiabatic ionization potentials (IP_A) are calculated in a similar way, but the total energies and ZPEs of the fully optimized, singly positively charged and neutral clusters are used instead. The location of the electron hole within positively charged clusters is inferred using spin density analysis. This may provide further information about the stability of a cluster structure with respect to the introduction of an electron hole in it, which may also be important for water photooxidation applications.

3. Results and Discussion

For convenience, the optimized structures are labeled by the number of TiO_2 units followed by a letter to distinguish the stability order, while the point group symmetries are given in parentheses. For example, the most and second most stable $(TiO_2)_{10}$ clusters are labeled as **10a** (C_2) and **10b** (C_{2v}), respectively, and so on. In the bonding analysis below we assume that one Ti−O bond exists if the Ti−O distance is smaller than 2.15 Å and that one Ti−Ti bond exists if the Ti−Ti distance is smaller than 2.90 Å. For comparison, the shortest bonding Ti−O and nonbonding Ti···Ti distances in rutile are 1.95 and 2.96 Å, respectively.[3,4,26] Such Ti−Ti bonds mainly exist within most TiO_2Ti four-membered rings, with Ti−Ti bond lengths of ∼2.8 Å, as also found previously for smaller $(TiO_2)_n$ clusters.[38] For clarity, not all possible Ti−Ti bonds within $(TiO_2)_n$ clusters are shown in the figures. The coordination number of a Ti or O atom is defined as the number of its surrounding Ti−O bonds and will be given in parentheses by a superscript when we discuss the bonding features of a specific atom. For example, $Ti^{(5)}$ and $O^{(3)}$ stand for 5-coordinated Ti and 3-coordinated O atoms, respectively.

3.1. Neutral Singlet $(TiO_2)_n$ Nanoparticles with $n = 10-16$. The optimized geometries of the three most stable structures are shown in Figure 1 for each n value, along with the ZPE-corrected relative energies (eV) with respect to the most stable neutral structure found in this work for each n value. In general, the $(TiO_2)_n$ clusters tend to form sphere- or rodlike compact structures. With 10−16 TiO_2 units, the optimized particle sizes may vary between about 0.9 and 1.5 nm dependent on the cluster shape, as estimated from the largest O···O distances within each cluster and the O atom covalent radius of about 0.7 Å, with most Ti and O atoms exposed on the particle surface as 4-coordinated $Ti^{(4)}$ and 2-coordinated $O^{(2)}$ atoms with covalent (or semicovalent) Ti−O single bonds of about 1.8−2.1 Å between them. Actually, such structural features of tetrahedral $Ti^{(4)}$ and bridging $O^{(2)}$ are very common for small $(TiO_2)_n$ clusters,[37,38] for which they may reduce structural tension. In fact, as can be seen from Figure 1, the most stable $(TiO_2)_n$ clusters with even $n = 10$, 12, 14, and 16 possess only $Ti^{(4)}$ and $O^{(2)}$ atoms, even when we start from some structures cut directly from TiO_2 bulk. On the other hand, for the $(TiO_2)_n$ clusters with odd $n = 11$, 13, and 15 the network with pure $Ti^{(4)}$ and $O^{(2)}$ would lead to somewhat planar $Ti^{(4)}$ sites, which may accept more oxygen ligands, and therefore, they tend to form more ionic structural features such as octahedral $Ti^{(6)}$ and pyramidal $Ti^{(5)}$.

Let us discuss $(TiO_2)_n$ clusters with even n values first. For the $(TiO_2)_{10}$ cluster, the most stable structure, **10a** (C_2), has only $Ti^{(4)}$ and $O^{(2)}$ atoms, with two additional loose Ti···O interactions at distances of 2.191 Å leading to the C_2 rather than higher C_{2v} point group symmetry. The second stable structure, **10b** (C_{2v}), as characterized by four $Ti^{(5)}$ atoms, two $O^{(3)}$ atoms, and one $O^{(4)}$ atom, was suggested[37] to represent the global minimum of the $(TiO_2)_{10}$ cluster, but is found to be 0.09 eV higher in energy than the new structure **10a**. We have located the transition state between structures **10a** and **10b** by changing the $O^{(4)}$ atom into an $O^{(2)}$ atom and taken the difference between the ZPE-corrected total energies of the transition state and structure **10b** to estimate the conversion barrier. In fact, the more compact structure **10b** is rather flexible with a very small (**10b** → **10a**) conversion barrier of about 0.08 eV. The third stable structure, **10c** (C_s), is characterized by three $Ti^{(5)}$ atoms, two $O^{(3)}$ atoms, and one $O^{(4)}$ atom, and it is 1.24 eV higher in energy. Despite some effort, we could not find other stable Ti═O defect-free structures that are even lower in energy than structure **10c** though it seems quite high in energy as compared to **10a**. For the $(TiO_2)_{12}$ cluster, all three most stable structures, **12a** (D_{2d}), **12b** (D_{2h}), and **12c** (D_{2h}), possess only $Ti^{(4)}$ and $O^{(2)}$ atoms, with the latter two being 0.75 and 0.76 eV higher in energy than the former one, respectively. Note that structure **12c** was initially constructed as an anatase-like structure with four $Ti^{(5)}$ and four $O^{(3)}$ atoms, but in its final geometry contains only $Ti^{(4)}$ and $O^{(2)}$ atoms to reduce structural tension. The global minimum for the $(TiO_2)_{12}$ cluster (Figure 1, 12d) suggested in ref 37, which is characterized by one $Ti^{(6)}$ atom, one $Ti^{(5)}$ atom, four $O^{(3)}$ atoms, and two terminal $O^{(1)}$ atoms, is found to be 2.21 eV higher in energy than structure **12a**.

The two most stable $(TiO_2)_{14}$ structures, **14a** (C_{2v}) and **14b** (C_{2v}), possess only $Ti^{(4)}$ and $O^{(2)}$ atoms, being 1.85 and 1.68 eV lower in energy than the third structure, **14c** (C_1), which is characterized by four $Ti^{(5)}$ and four $O^{(3)}$ atoms. The previously suggested[37] $(TiO_2)_{14}$ global minimum (Figure 1, 14d) was characterized by one $Ti^{(6)}$ atom, four $Ti^{(5)}$ atoms, and six $O^{(3)}$ atoms and has a more compact structure, but it is 2.53 eV higher in energy than **14a**.

The three most stable $(TiO_2)_{16}$ structures, **16a** (D_{2d}), **16b** (D_{2d}), and **16c** (C_{2v}), are characterized by only $Ti^{(4)}$ and $O^{(2)}$ atoms, with the latter two being 0.46 and 0.68 eV higher in energy than the former one, respectively. We have also found the previously suggested[39] $(TiO_2)_{16}$ nanocrystal structure (Figure 1, 16d) cut from TiO_2 anatase bulk and characterized by four $Ti^{(5)}$ and four $O^{(3)}$ atoms without a net dipole moment and with all Ti and O atoms being at least 4- and 2-coordinated, respectively. However, this somewhat "hollow" structure (Figure 1) is rather unstable with respect to the lowest energy structure **16a** (its energy being higher by 5.94 eV), making it questionable that this cluster would be "the smallest possible nanocrystal" of TiO_2. In short, the lowest energy, stable $(TiO_2)_n$ clusters found here, with even $n = 10$, 12, 14, and 16, tend to form compact networks of a semicovalent nature, with mainly tetrahedral $Ti^{(4)}$ and bridging $O^{(2)}$ atoms. The pair-potential model[37] seems to be inappropriate for predicting the structures of TiO_2 clusters with a semicovalent nature; i.e., the existing model is not accurate enough to predict global minimum energy structures for these clusters.

Now let us discuss $(TiO_2)_n$ clusters with odd n values. For the $(TiO_2)_{11}$ cluster, the most stable structure, **11a** (C_1), is characterized by one $Ti^{(6)}$ atom, one $Ti^{(5)}$ atom, and three $O^{(3)}$ atoms, while the second structure, **11b** (C_s), is characterized by three $Ti^{(5)}$ and three $O^{(3)}$ atoms and is 0.23 eV higher in energy. Structure **11c** (C_1) closely resembles the global minimum structure suggested in ref 37 with one highly coordinated $Ti^{(7)}$ atom, two $Ti^{(5)}$ atoms, five $O^{(3)}$ atoms, and one terminal $O^{(1)}$ atom, but it is found to be 0.61 eV higher in energy than **11a**.

For the $(TiO_2)_{13}$ cluster, the most stable structure by far, **13a** (C_{2h}), is characterized by one $Ti^{(6)}$ atom in the cluster center

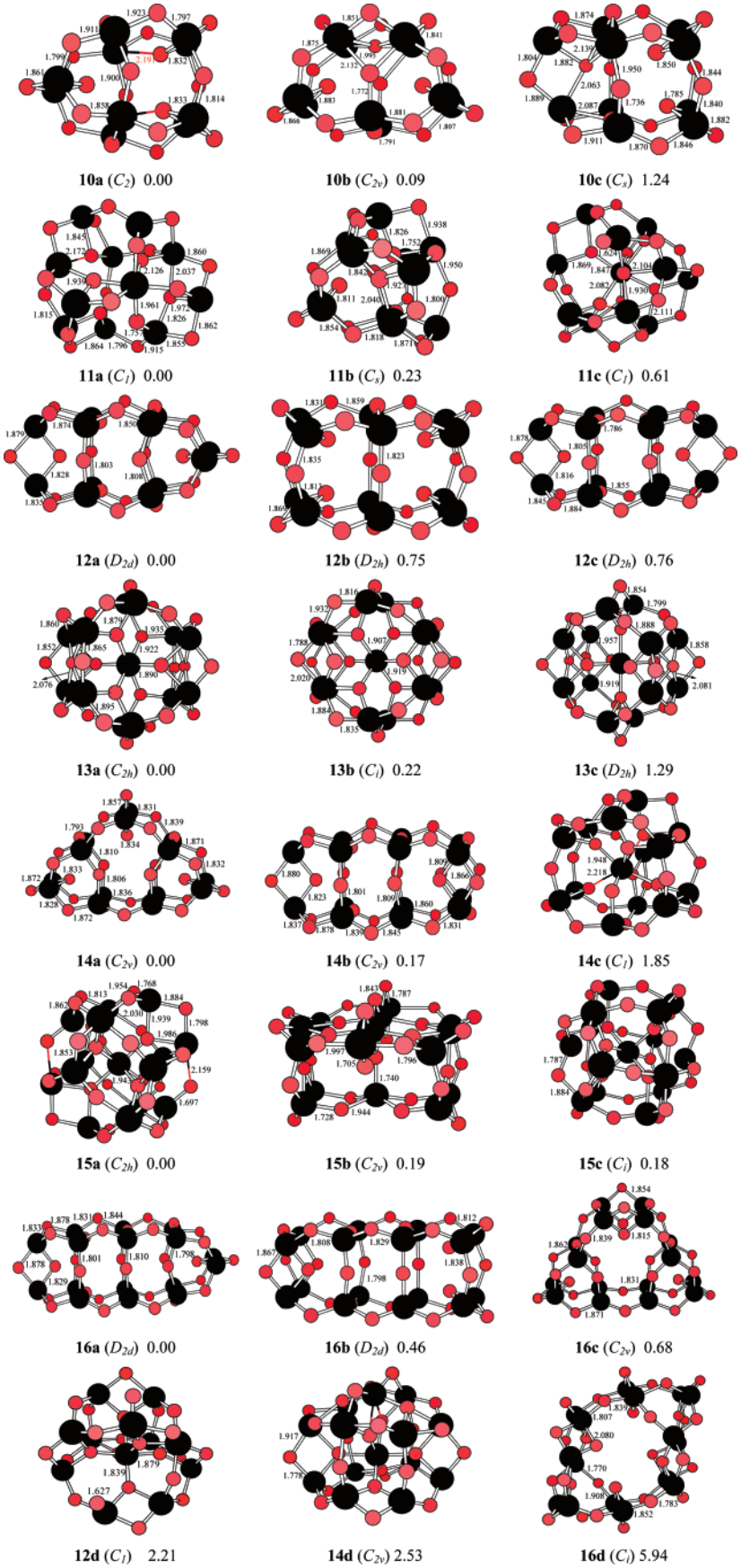

Figure 1. Geometries of stable neutral singlet $(TiO_2)_n$ nanoclusters with $n = 10-16$ along with the ZPE-corrected relative energies (eV) with respect to the most stable neutral structure found in this work for each n value. The Ti═O double and Ti−O single bonds are assumed to be shorter than 1.66 and 2.15 Å, respectively. Ti−Ti bonds (shorter than 2.90 Å) may also exist within the TiO_2Ti four-membered ring but are not shown for clarity. The Ti and O atoms are shown as black and red balls, respectively, and the colors are varied by depth with a ratio of 40%. Loose Ti···O bonds are indicated by dashed lines in half black and half red.

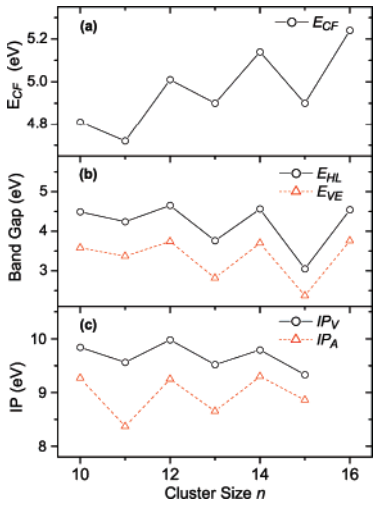

Figure 2. Odd−even oscillation of various electronic properties of the most stable $(TiO_2)_n$ clusters as a function of cluster size n: **(a)** for the cluster formation energies E_{CF} (eV); **(b)** for the band gaps (eV) estimated from the HOMO−LUMO gap E_{HL} and from the vertical excitation energy E_{VE}; (c) for the vertical and adiabatic ionization potentials (IP_V and IP_A, eV).

surrounded by six $O^{(3)}$ atoms, along with eight $Ti^{(5)}$ and two *planar* $O^{(4)}$ atoms. Remarkably, each of the two 4-coordinated planar $O^{(4)}$ atoms is closely surrounded by four $Ti^{(5)}$, four $O^{(2)}$, and three $O^{(3)}$ atoms. As will be discussed later, such chemical environments strongly destabilize the lone pair of $O^{(4)}$ atoms and thus lead to a very small band gap (or excitation energy). Attempts to replace the planar $O^{(4)}$ atoms by bridging $O^{(2)}$ atoms lead to structure **13b** (C_i) with two evidently different Ti−O bond lengths of 1.788 and 2.020 Å involving the new $O^{(2)}$ atom, which is 0.22 eV higher in energy than **13a**. The resultant structure **13b** is characterized by one $Ti^{(6)}$ atom surrounded by six $O^{(3)}$ atoms and further by four $Ti^{(5)}$ atoms, in addition to other $Ti^{(4)}$ and $O^{(2)}$ atoms. The highly symmetric structure **13c** (D_{2h}) is obtained by changing the orientation of six $O^{(3)}$ atoms of structure **13a**, but it is found to be 1.29 eV higher in energy.

For the $(TiO_2)_{15}$ cluster, the optimized structure **15a** (C_{2h}) closely resembles the suggested[37] global minimum from the pair-potential model, which is characterized by one octahedral $O^{(6)}$ atom in the center and four $Ti^{(5)}$, two $Ti^{(3)}$, six $O^{(3)}$, and two $O^{(1)}$ (within Ti═O···Ti structures) atoms. Interestingly, structure **15b** (C_{2v}) is constructed from rutile bulk directly, represents the smallest defect-free TiO_2 rutile nanocrystal found so far, and is characterized by two $Ti^{(6)}$, three $Ti^{(5)}$, and four $O^{(3)}$ atoms. It is only 0.19 eV higher in energy (or 0.013 eV per TiO_2 unit) than **15a**, and therefore, it could be very useful for further mechanistic studies such as the adsorption structures of water and its photooxidation intermediates on rutile nanoparticles. Another stable structure that avoids the terminal Ti═O···Ti features found in **15a**, structure **15c** (C_i), is characterized by one $O^{(6)}$ atom in the center and four $Ti^{(5)}$, two $Ti^{(3)}$, and six $O^{(3)}$ atoms. It is 0.07 eV higher in energy than **15b** before ZPE correction but becomes 0.01 eV lower in energy after ZPE correction. In short, stable $(TiO_2)_n$ clusters with odd $n = 11$, 13, and 15 tend to form compact networks with ionic features as characterized by one or two octahedral $Ti^{(6)}$ centers and $Ti^{(5)}$ and $O^{(3)}$ atoms. The pair-potential model[37] performs better at predicting structures with these ionic features, perhaps because it is biased to do so, being developed to reproduce bulk rutile.

For a comparison of the stabilities of $(TiO_2)_n$ clusters, we have collected the cluster formation energies $E_{CF}[(TiO_2)_n]$ (per TiO_2 unit from an isolated TiO_2 molecule) in Table 1. It can be

TABLE 1: B3LYP/LANL2DZ-Calculated Cluster Formation Energies per TiO_2 Unit without and with ZPE Correction (E_{CF-ZPE} and E_{CF}), HOMO−LUMO Gaps (E_{HL}), Vertical (IP_V) and Adiabatic (IP_A) Ionization Potentials, and TDDFT/B3LYP Vertical Excitation Energies (E_{VE}) and Singlet−Triplet Gaps (E_{ST}) for the Most Stable Structures of $(TiO_2)_n$ with $n = 10-16$[a]

structure	E_{CF-ZPE}	E_{CF}	E_{HL}	E_{VE}	E_{ST}	IP_V	IP_A
10a	4.81	4.73	4.49	3.58	3.53	9.84	9.27
10b	4.80	4.72	4.15	3.18	3.15	9.52	9.18
11a	4.72	4.64	4.24	3.37	3.26	9.56	8.37
12a	5.01	4.93	4.65	3.74	3.68	9.98	9.25
13a	4.90	4.83	3.76	2.82	2.80	9.52	8.65
13b	4.89	4.81	3.44	2.48	2.36		
14a	5.14	5.06	4.56	3.70	3.66	9.79	9.30
15a	4.90	4.83	3.05	2.37	2.37	9.33	8.86
15b	4.90	4.82	4.25	3.51	3.47	9.46	8.57
16a	5.24	5.16	4.54	3.76	3.72		
rutile		6.62		3.0			
(anatase)		(6.57)[b]		(3.2)[c]			

[a] All energy data are in units of electronvolts. The total energy of the free TiO_2 molecule is −208.584423 hartrees, and the corresponding zero-point energy is 0.005411 hartree. [b] References 53−55. [c] Reference 11.

seen that the E_{CF} values of the most stable Ti═O defect-free structures tend to increase with the cluster size n from 4.73 eV (**10a**) to 5.16 eV (**16a**). For clarity, the E_{CF} values of the most stable $(TiO_2)_n$ clusters as a function of cluster size n are plotted in Figure 2a. An interesting odd−even oscillation of the E_{CF} values is observed, with the even-n clusters being energetically favored by at least 0.09 eV per TiO_2 unit. Another important observation is that for all the $(TiO_2)_n$ clusters with $n = 10-16$ the ZPE corrections to the E_{CF} values (about 0.08 eV per TiO_2 unit) are almost constant. This suggests a useful way to include ZPE corrections for larger TiO_2 nanoparticles, for which frequency analysis may be too expensive or even unfeasible.

From the experimental standard formation enthalpies[53,54] of the TiO_2 molecule (−305.43 kJ/mol) and of TiO_2 bulk (rutile, −944.0 ± 0.8 kJ/mol),[55] the E_{CF} value of TiO_2 bulk can be evaluated as about 6.62 eV per TiO_2 unit, which is still about 1.98−1.46 eV larger than those of the $(TiO_2)_n$ nanoparticles with $n = 10-16$. Assuming a spherical shape, the diameters of the largest $(TiO_2)_{16}$ and smallest $(TiO_2)_{10}$ nanoclusters in this work are about 1.1 and 0.9 nm, respectively, leading to estimated surface formation energies in the range of 0.6−1.2 J/m^2 if the E_{CF} differences between TiO_2 bulk and nanoparticles are ascribed only to surface formation. Interestingly, the estimated nanocluster surface formation energies are quite close to the experimentally estimated surface enthalpies of 2.2 and 0.4 J/m^2 for rutile and anatase nanoparticles with diameter >7 nm, respectively.[25] This lends further support to the idea that $(TiO_2)_n$ nanoclusters without Ti═O defects may be useful for modeling reactions on TiO_2 surfaces and specific sites such as corners and steps.

3.2. Infrared Spectra of Stable $(TiO_2)_n$ Nanoparticles with $n = 10-16$. Figure 3 shows the calculated infrared spectra of the most stable $(TiO_2)_n$ clusters found in this work. Note that the theoretical vibrational frequencies are scaled by a factor of 0.95 on the basis of a comparison between theoretical and experimental frequencies of TiO and TiO_2 molecules[38] and that only the relative intensities of allowed electric dipole transitions are shown in the predicted spectra. One common feature of the spectra of all new stable clusters with $n = 10-16$ is that they do not exhibit a transition peak around 1020 cm^{-1} that is due to stretching of terminal Ti═O, as found for small $(TiO_2)_n$ clusters.[38] For even n values the stable $(TiO_2)_n$ clusters contain

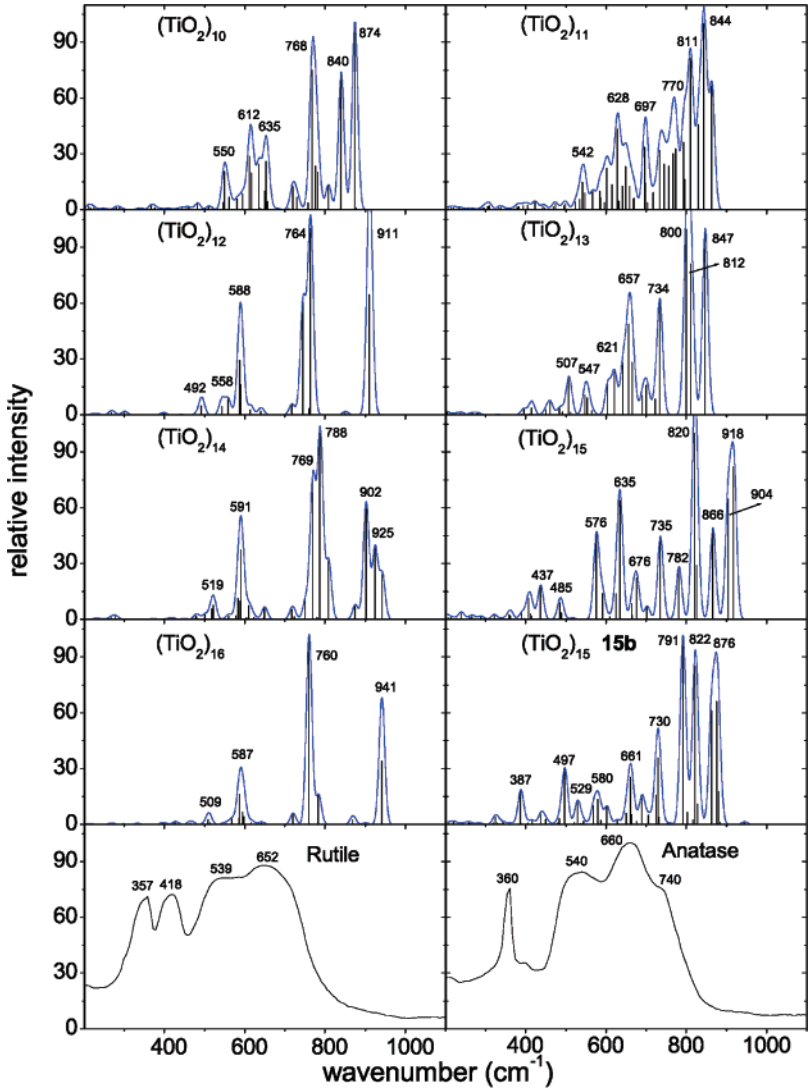

Figure 3. Infrared spectra of the most stable $(TiO_2)_n$ nanoclusters with $n = 10-16$. The B3LYP/LANL2DZ-calculated vibrational frequencies (cm^{-1}) are scaled by a factor of 0.95, while the intensities are relative to that of the strongest vibrational transition (taken as 100). The blue lines show the spectral envelopes, with each stick being broadened as a Gaussian function with a width of 10 cm^{-1}. The spectra of bulk rutile and anatase (ref 54) are included for comparison.

only $Ti^{(4)}$ and $O^{(2)}$ atoms, and thus, the infrared spectra are relatively simple and quite similar to each other, with mainly three strong transition groups due to the symmetric and antisymmetric stretching modes of Ti−O−Ti around 590 cm^{-1} and around 770 and 920 cm^{-1}, respectively. Note that the antisymmetric stretching modes of low and high frequency are due to bent Ti−O−Ti moieties (with a bond angle around 100−120°) and to quasi-linear Ti−O−Ti moieties (with a bond angle greater than 140°), respectively. As an exception, the spectrum of the $(TiO_2)_{10}$ **10a** cluster shows some extra structure, mainly due to its low point group symmetry and two additional loose Ti···O (2.191 Å) bonds (see Figure 1) with some $Ti^{(5)}$ and $O^{(3)}$ character. In fact, the strong vibrational peaks around 635 and 840 cm^{-1} of $(TiO_2)_{10}$ **10a** are very similar to those observed for the stable $(TiO_2)_n$ clusters with odd n values as will be discussed below. Even then, the strong peak at 768 cm^{-1} still remains for cluster **10a**. Thus, the characteristic peak close to 770 cm^{-1} can be useful for probing surface bridging Ti−O−Ti structures.

The stable $(TiO_2)_n$ clusters with odd n values may contain additional $Ti^{(6)}$, $Ti^{(5)}$, $O^{(3)}$, and $O^{(4)}$ atoms, and thus, their infrared spectra are more complicated. Among these TiO_2 nanoclusters, $(TiO_2)_{15}$ **15b** represents the only stable and Ti═O defect-free TiO_2 (rutile) nanocrystal found in this work. It is thus interesting to compare its infrared spectrum with the experimental[54] ones of both rutile and anatase bulk. As can be seen from Figure 3, the $(TiO_2)_{15}$ **15b** cluster shows some strong peaks around 387, 497, 580, 661, and 730 cm^{-1}, which are comparable to the broad absorptions of rutile around 357, 418, 539, and 652 cm^{-1} and of anatase around 360, 540, 660, and 740 cm^{-1}. In-depth analysis of the $(TiO_2)_{15}$ **15b** spectrum shows that the 387 and 497 cm^{-1} peaks are related mainly to out-of-plane modes of 3-coordinated $O^{(3)}$, the 580, 661, and 822 cm^{-1} peaks to in-plane modes of $O^{(3)}$, and the 730, 791, and 876 cm^{-1} peaks to antisymmetric Ti−O−Ti stretching modes with minor contributions from $O^{(3)}$.

Similarly, strong peaks due to $O^{(3)}$ vibrations around 660 and 820 cm^{-1} are also observed for all other stable odd-n $(TiO_2)_n$ clusters, in addition to the strong features of antisymmetric Ti−O−Ti stretching around 735 and 790 cm^{-1} and above 840 cm^{-1}. Note that the vibrational peak around 790 cm^{-1} is blue-shifted by about 20 cm^{-1} as compared with the corresponding vibrational feature observed for even-n clusters, suggesting a different chemical environment of the Ti atoms. At a level of greater detail, a strong side peak around 904 cm^{-1} is observed for the $(TiO_2)_{15}$ **15a** cluster due to antisymmetric stretching

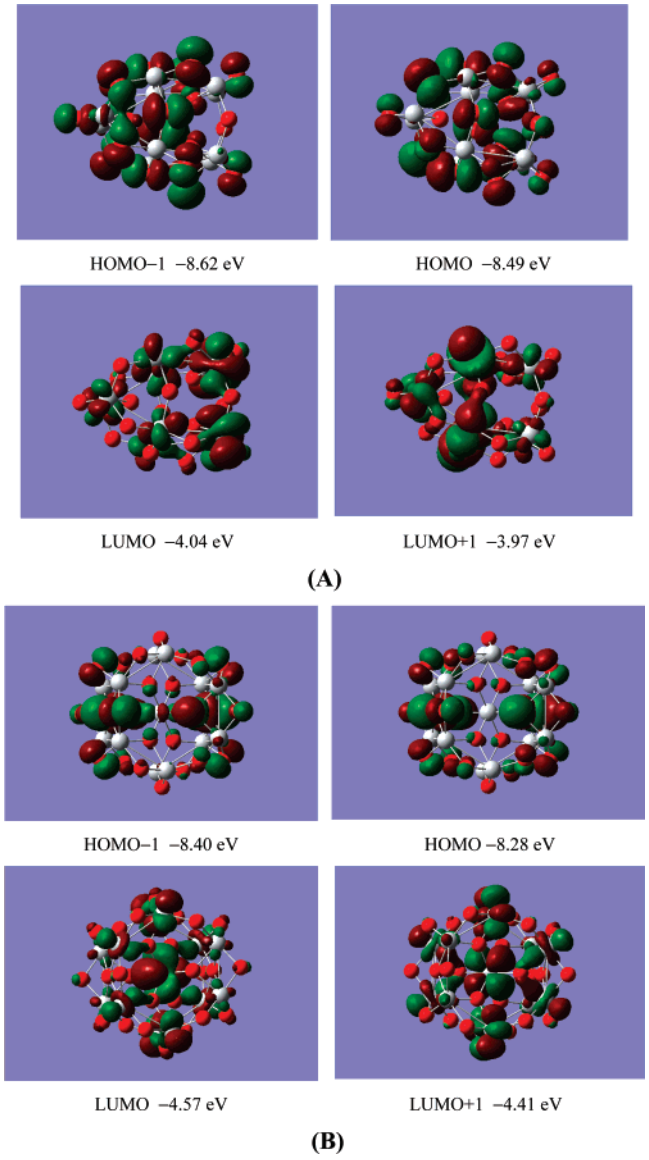

Figure 4. Frontier molecular orbitals of the stable clusters: **(**A**)** $(TiO_2)_{10}$ **10a** and **(**B**)** $(TiO_2)_{13}$ **13a**. These include the highest and next highest occupied (HOMO and HOMO − 1) and the lowest and next lowest unoccupied (LUMO and LUMO + 1) molecular orbitals for each cluster. The molecular skeletons are shown as ball−stick models, with the gray and red balls being Ti and O atoms, respectively. The wave functions are plotted at an absolute isovalue of 0.02 au in brown and green for the positive and negative parts, respectively. The orbital energy levels at the B3LYP/LANL2DZ level are also shown in electronvolts.

modes of Ti═O···Ti bonding, while the vibrations involving $O^{(4)}$ atoms for the $(TiO_2)_{13}$ **13a** cluster are combined into the peaks around 734 and 800 cm^{-1} mainly due to antisymmetric modes also involving $O^{(2)}$ and $O^{(3)}$ atoms. Since the bulk TiO_2 absorption peaks are all below 740 cm^{-1}, the characteristic strong infrared peak around 820 cm^{-1} observed for odd-*n* clusters can be useful for identifying surface $O^{(3)}$ species.

3.3. Electronic Properties of Stable $(TiO_2)_n$ Nanoparticles with $n = 10-16$. Figure 4 shows the frontier molecular orbitals (FMOs) including HOMO − 1, HOMO, LUMO, and LUMO + 1 of two stable $(TiO_2)_n$ nanoclusters, **10a** and **13a**. For each cluster, the occupied FMO levels are found to be very close to each other within 0.13 eV, and the same applies for the unoccupied FMO levels. It can be seen that the occupied and unoccupied FMOs, which can be related to the valence and conduction bands in the case of bulk TiO_2, consist almost exclusively of the O(2p) lone pairs and empty Ti(3d) atomic orbitals, respectively. Moreover, both the occupied and unoccupied FMOs are quite delocalized with respective contributions from many O or Ti atoms, suggesting the delocalized nature of vertical excitations of $(TiO_2)_n$ nanoclusters. However, it should be pointed out that the electron and hole created upon *vertical* photoexcitation may be stabilized and trapped (localized) on one or two surface Ti and O atoms, respectively, after further structural relaxation.

In Table 1, we have also collected some useful electronic properties of the stable $(TiO_2)_n$ clusters such as the HOMO−LUMO gaps (E_{HL}), the vertical excitation energies to both the lowest singlet (E_{VE}) and triplet excited (E_{ST}) states, and the vertical (IP_V) and adiabatic (IP_A) ionization potentials. Since the defect-free $(TiO_2)_{15}$ **15b** nanocrystal closely resembles the rutile bulk structure, we take it as the reference structure for most discussion about the electronic properties of ∼1 nm TiO_2 nanoparticles here. Let us discuss the calculated E_{HL} values at first, with that of the defect-free **15b** nanocrystal (4.25 eV) as the reference value. The E_{HL} values of the most stable $(TiO_2)_n$ clusters with even $n = 10$, 12, 14, and 16 are more or less constant around 4.5−4.6 eV, i.e., about 0.3 eV larger than that of **15b** (Table 1 and Figure 2b). On the other hand, the E_{HL} values of 4.24 (**11a**), 3.76 (**13a**), 3.44 (**13b**), and 3.05 (**15a**) eV of odd-*n* $(TiO_2)_n$ clusters are at least 0.3 eV smaller than those of the even-*n* clusters. Specifically, though the E_{HL} value of the **11a** cluster is very close to that of the **15b** nanocrystal, those of **13a**, **13b**, and **15a** clusters are surprisingly smaller by about 0.5, 0.8, and 1.2 eV. Close examination of the structures (Figure 1) and FMOs (Figure 4) suggests that the surprisingly small E_{HL} values could be due to the shortest $O^{(4)}\cdots O^{(3)}$ distances of 2.30 Å within **13a**, the shortest $O^{(2)}\cdots O^{(2)}$ distances of 2.34 Å connecting somewhat distorted $Ti^{(5)}$ centers within **13b**, and the defective $Ti^{(3)}$═$O\cdots Ti^{(4)}$ sites within **15a** clusters, on which the holes within the corresponding positively charged clusters tend to be localized as will be discussed further in section 3.4.

Usually, the E_{HL} values are directly related to the lowest vertical excitation energies (E_{VE}) and/or the band gap of nanoparticles, which however could lead to large deviation if the lowest excited states are of multiconfiguration nature. For singlet close-shell $(TiO_2)_n$ clusters, the TDDFT/B3LYP method is expected to give reliable excitation energies, at least for the lowest several excited states. As can be seen from Table 1 and Figure 2b, the TDDFT E_{VE} values are consistently about 0.7−1.0 eV smaller than the corresponding E_{HL} values, which can be due to the multiconfiguration nature of the excited-state wave functions as confirmed by a close examination of the largest coefficients in the CI expansion. Furthermore, the lowest vertical singlet−triplet gaps (E_{ST}) are very close (within 0.1 eV) to the corresponding E_{VE} values, mainly due to the nature of the excitations almost being the same, with quite similar CI expansion coefficients. For example, the largest CI expansion coefficients are 0.622 (HOMO → LUMO + 1) and 0.687 (HOMO → LUMO) for the singlet excited **10a** and **13a** clusters and 0.633 (HOMO → LUMO + 1) and 0.675 (HOMO → LUMO) for the triplet excited **10a** and **13a** clusters, respectively. In both cases the transition probabilities (squares of CI coefficients) are roughly half rather than one to the main excited configurations. For this reason, the conventional HOMO−LUMO gap method may overestimate the band gaps of TiO_2 nanoparticles.

To avoid very expensive TDDFT calculations on many excited states for large $(TiO_2)_n$ clusters, a reasonable density of states may be obtained by shifting the B3LYP-calculated

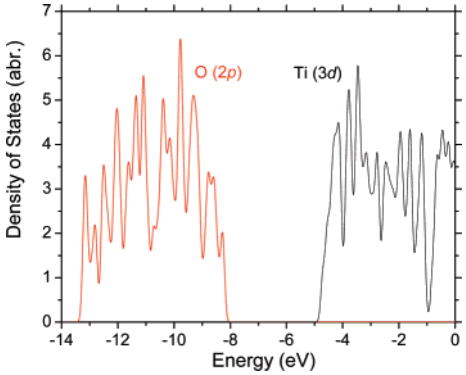

Figure 5. B3LYP/LANL2DZ-calculated density of states for the $(TiO_2)_{15}$ **15b** nanocrystal with a band gap of about 3.5 eV. The upper part of the valence band (in red) and the lower part of the conduction band (in black) are shown, for which the states consist mainly of occupied O(2p) and unoccupied Ti(3d) atomic states. The conduction band has been shifted down by 0.7 eV according to TDDFT results, and all energy levels have been broadened as a Gaussian function of width 0.1 eV to obtain the density of states.

unoccupied orbital levels down and slightly broadening each level with an appropriate width. As an example, in Figure 5 we show the calculated density of states for the $(TiO_2)_{15}$ **15b** nanocrystal with a band gap of about 3.5 eV. The conduction band has been shifted down by 0.7 eV according to the TDDFT results, and all energy levels have been broadened by convoluting with a Gaussian function of width 0.1 eV to obtain the density of states. The upper part of the valence band and the lower part of the conduction band consist mainly of occupied O(2p) electron lone pairs and unoccupied Ti(3d) atomic orbitals. For small TiO_2 nanoparticles, the calculated density of states shows many sharp features, which would most likely be smoothed out for large nanocrystals.

Consistent with the expected quantum-size effects, the E_{VE} (3.51 eV) of the $(TiO_2)_{15}$ **15b** rutile nanocrystal is about 0.3−0.5 eV larger than the experimental TiO_2 bulk band gaps of 3.0−3.2 eV.[11] The E_{VE} values of the most stable even-n $(TiO_2)_n$ clusters are more or less constant around 3.7 eV, similar to the value for **15b**. This can be due to two reasons: first, the quantum-size effect for the nanoparticles studied here should be almost the same due to quite similar cluster diameters around 1 nm; second, with only tetrahedral $Ti^{(4)}$ and bridging $O^{(2)}$ atoms the electronic structures of these clusters are expected to be quite similar. Although the E_{VE} value of 3.37 eV of **11a** is very close to that of the **15b** nanocrystal, those of the **13a**, **13b**, and **15a** clusters are surprisingly smaller by 1.03, 0.69, and 1.14 eV than that of the **15b** nanocrystal, respectively, due to the small O···O distances within **13a** and **13b** and the defective $Ti^{(3)}$═O···$Ti^{(4)}$ sites within **15a** as discussed above. The fact that the E_{VE} values of stable even-n $(TiO_2)_n$ clusters are about 0.2 eV larger than stable defect-free **11a** and **15b** clusters can be due to the O(2p) → Ti(3d) character of the (lowest) excitations within $(TiO_2)_n$ nanoclusters. The 2p lone pairs of bridging $O^{(2)}$ atoms are more stable than those of planar $O^{(3)}$ from simple consideration of least repulsion of hybrid orbitals, while the (lowest) Ti(3d) orbital of octahedral $Ti^{(6)}$ should be more stable than the lowest 3d orbital of tetrahedral $Ti^{(4)}$ due to the smaller tetrahedral crystal field splitting. Thus, the larger E_{VE} values of even-n $(TiO_2)_n$ clusters are due to more stable O(2p) lone pairs and less stable Ti(3d) orbitals.

3.4. Positively Charged $(TiO_2)_n^+$ Nanoparticles with n = 10−16. As can be expected from the rather delocalized HOMOs of neutral $(TiO_2)_n$ clusters (see Figure 4), the electron holes are found to be delocalized over the whole positively charged

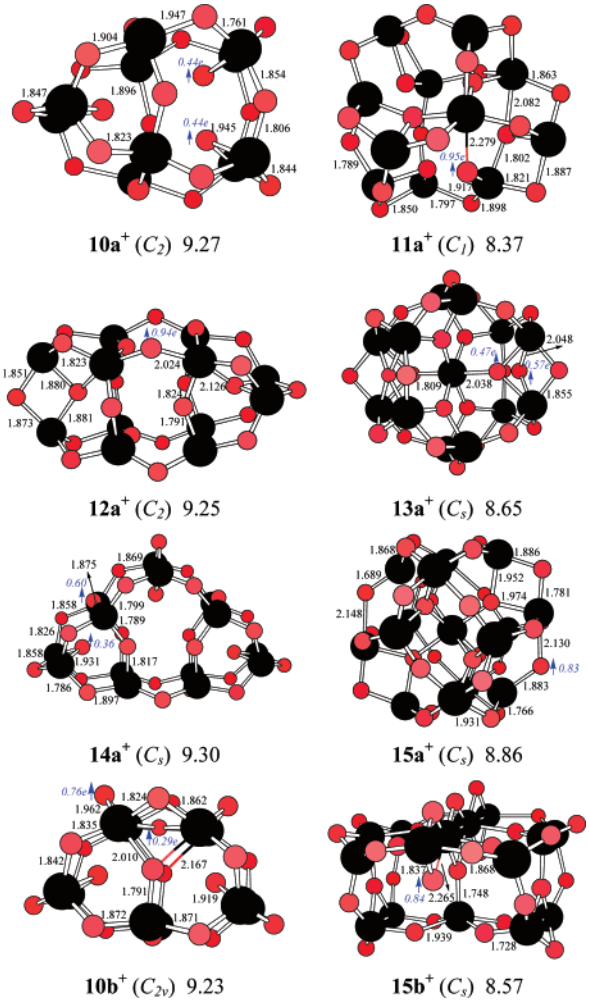

Figure 6. Geometries of positively charged doublet $(TiO_2)_n^+$ nanoclusters with $n = 10-16$, along with the ZPE-corrected relative energies (eV) with respect to the most stable neutral structure found in this work for each n value. The location of the main atomic spin densities (larger than 0.2 e) is indicated by blue arrows and blue italic numbers. The other details are the same as in Figure 1.

$(TiO_2)_n^+$ clusters upon vertical ionization, with the respective largest spin densities on single oxygen atoms being only 0.19, 0.13, 0.11, and 0.17 e within the **12a**$^+$, **14a**$^+$, **15a**$^+$, and **15b**$^+$ clusters. As can be seen from Table 1 and Figure 2c, the calculated vertical ionization potentials, IP_V, are quite high between 9.3 and 10 eV. Again, the IP_V values show interesting odd−even oscillations (Figure 2c), with those of even-n clusters being about 0.3 eV higher than those of odd-n clusters, which can be related to the stability order of O(2p) lone pairs as discussed above in section 3.3.

Figure 6 shows some fully relaxed positively charged $(TiO_2)_n^+$ clusters, which could be very useful to model the reaction of H_2O with surface-trapped holes. In general, after full structural relaxation, the $(TiO_2)_n^+$ clusters adopt a somewhat reduced point group symmetry as compared with the corresponding singlet neutral clusters, and the electron holes are found to be quite localized, mainly on only one or two $O^{(2)}$ atoms rather than on $O^{(3)}$ atoms. As the main consequence, the Ti−O bonds involving the O atom with the hole on it tend to be elongated by about 0.1−0.2 Å. For stable even-n $(TiO_2)_n^+$ clusters the situation is relatively simple since only $O^{(2)}$ atoms are present: the holes tend to be localized on one bridging $O^{(2)}$ within **12a**$^+$ or on two $O^{(2)}$ atoms within **10a**$^+$ and **14a**$^+$ when close interatomic O(2p) lone pair interactions (i.e., within short

distance, <2.4 Å) are possible that may stabilize the hole. For stable odd-n $(TiO_2)_n^+$ clusters the situation is more complicated since more atomic oxygen types are present. The holes are found to be localized mainly on one $O^{(2)}$ atom within the defect-free **11a**$^+$ and **15b**$^+$ clusters. The holes are localized between one $O^{(2)}$ (the original $O^{(4)}$ of neutral **13a**) and its nearest $O^{(3)}$ neighbor within **13a**$^+$ and on one Ti═O···Ti site within **15a**$^+$. Interestingly, the hole is localized mainly on one $O^{(2)}$ and one $O^{(4)}$ rather than on $O^{(3)}$ atoms within **10b**$^+$, without an accompanying change of an $O^{(4)}$ into an $O^{(2)}$ atom as found in the **13a**$^+$ cluster. Note that, in all cases, the localization of the hole does not change the overall cluster structure though some local changes of bond lengths to the hole are observed and the point group symmetry may be lower, suggesting the usefulness of our new $(TiO_2)_n$ nanoclusters for modeling the surface reactions of surface-trapped holes with reactants such as water and organic pollutant.

As can be seen from Table 1 and Figure 2c, the calculated adiabatic ionization potentials (IP_A) of some stable $(TiO_2)_n$ clusters may vary between 8.3 and 9.3 eV, showing also odd−even oscillations (see Figure 2c). The IP_A values are about 0.5−1.2 eV smaller than the corresponding IP_V values, showing that structural relaxation helps to both stabilize and localize surface-trapped holes: the holes are quite delocalized over the $(TiO_2)_n$ nanoparticles upon vertical ionization (or excitation), but they are localized mainly on one or two oxygen atoms after structural relaxation (i.e., hole trapping). By assuming the structure with a delocalized hole on it as the "transition state", the differences between IP_V and IP_A values may be taken as the upper bound for the diffusion barriers of surface-trapped holes on bare TiO_2 surfaces. This implies a hole diffusion barrier of at most 0.5−1.2 eV.

3.5. Implications for Photooxidation of H_2O and Photochemistry on TiO_2. Due to the large band gap of about 3.0−3.2 eV of bulk TiO_2, it absorbs only the ultraviolet part of the solar emission thus with limited efficiency. It would be very nice to develop new small band gap TiO_2 materials for important applications such as water photoelectrolysis. Recently, it has been shown that TiO_2 nanotube and amorphous TiO_2 materials may exhibit some visible light activity in photocatalytic reactions,[21,22] though the nature of the active sites is still unknown. Interestingly, we have found some stable odd-n $(TiO_2)_n$ nanoparticles with quite small band gaps such as **13a**, **13b**, and **15a**. The key structural features responsible for the small band gaps are identified to be close interatomic O(2p) lone pair interactions and/or rather asymmetric Ti═O···Ti bonding. If such "metastable" features could be stabilized as "intrinsic" structures within new TiO_2 nanostructured materials, it could lead to small band gap TiO_2 photocatalysts with strong visible light activity. For example, perhaps the simultaneous synthesis of $(TiO_2)_n$ nanoparticles and conducting materials incorporating the nanoparticles could be engineered in such a way that a high proportion of small $(TiO_2)_n$ clusters with odd n would be incorporated into the material, which could then exhibit the desired visible light activity. To this end, further studies are still desired to verify whether the matrix-supported TiO_2 nanoparticles could exhibit small band gaps similar to those predicted for some gas-phase nanoparticles in this work.

In the recently proposed mechanism of water photooxidation on the TiO_2 surface,[24] it was suggested that the reaction should be initiated by a nucleophilic attack of a H_2O molecule on a surface-trapped hole $[Ti_2{=}O{-}Ti]^+_s$ localized on a 3-coordinated $O^{(3)}$ atom at a step or corner site, leading to an intermediate $[Ti{-}O^{\bullet}HO{-}Ti]_s$ radical:

$$[Ti_2{=}O{-}Ti]^+_s + H_2O \rightarrow [Ti{-}O^{\bullet}HO{-}Ti]_s + H^+ \quad (3)$$

It was further proposed that the slow reaction 3 found on atomically smooth TiO_2 surfaces such as rutile (110) and (100) is due to a larger activation energy for the insertion of OH into $[Ti_2{=}O{-}Ti]$ sites, which should be more rigid at a terrace than at a surface step or corner.

A revised water photooxidation mechanism involving surface-trapped holes at bridging $[Ti{-}O{-}Ti]_s$ sites may be proposed as follows:

$$[Ti{-}O{-}Ti]^+_s + H_2O \rightarrow [Ti{-}O^{\bullet}HO{-}Ti]_s + H^+ \quad (4)$$

This new mechanism is based on the following considerations. First, according to our calculations, the trapped holes may be localized on only one terminal $O^{(1)}$ atom if present or on one $O^{(2)}$ atom in cases where interatomic O(2p) lone pair interaction with another nearby O atom (<2.4 Å) is not possible. Since the shortest O···O distances that could favor interatomic O(2p) lone pair interaction within the TiO_2 rutile and anatase phases are more than 2.7 Å, the holes should be trapped on defective Ti═O sites on surfaces with defects or on bridging $O^{(2)}$ sites on defect-free surfaces. Second, surface bridging $[Ti{-}O{-}Ti]_s$ rather than terminal Ti═O sites are common on stable TiO_2 surfaces, and experiments show that H_2O is adsorbed molecularly at the predominant rutile (110) and anatase (101) surfaces, except at defect sites such as oxygen vacancies.[4] Third, bridging $[Ti{-}O{-}Ti]_s$ sites are more flexible for hole-trapping and insertion of a OH group than the more rigid $[Ti_2{=}O{-}Ti]$ sites. Due to their high reactivity, defective Ti═O sites might only exist as short-lived reactive intermediates rather than as stable surface species. From these considerations, the best cluster models for modeling reactions of surface-trapped holes on TiO_2 nanoparticles among those presented in this work could be **11a** and **15b**, since these clusters possess both bulklike $Ti^{(6)}$ and $O^{(3)}$ atoms and the bridging $O^{(2)}$ atoms on which the hole tends to localize. Studies of the water photooxidation mechanism on our novel cluster models are ongoing.

4. Conclusions

(1) The electronic structure and stability of $(TiO_2)_n$ nanoparticles with $n = 10-16$ have been investigated using the density functional B3LYP/LANL2DZ method, with special effort to find stable Ti═O defect-free structures.

(2) We find an interesting odd−even oscillation of the structural features and electronic properties of defect-free $(TiO_2)_n$ clusters: even-n clusters tend to form compact structures of more covalent nature that are more stable, with larger HOMO−LUMO gaps, vertical excitation energies, and ionization potentials, while odd-n clusters tend to form compact structures of more ionic nature that are less stable.

(3) The new half-spherical $(TiO_2)_{15}$ cluster **15b** represents the smallest defect-free rutile nanocrystal found so far, which is only slightly higher in energy than the spherical **15a** cluster with two defective Ti═O···Ti sites.

(4) Strong characteristic infrared peaks around 770 and 820 cm^{-1} could be very useful for identifying surface $O^{(2)}$ and $O^{(3)}$ species, respectively.

(5) The stablest clusters with odd n exhibit small vertical excitation energies, in some cases significantly smaller than the band gap of bulk TiO_2. This suggests that if materials can be engineered that incorporate such $(TiO_2)_n$ with odd and small n values, they could exhibit visible light photoactivity.

(6) Electron holes are localized on one bridging $O^{(2)}$ rather than on planar $O^{(3)}$ atoms on Ti═O defect-free TiO_2 surfaces, suggesting revision of a recently proposed water photooxidation mechanism involving surface-trapped holes on $O^{(3)}$ atoms. Studies of the water photooxidation mechanism on our novel cluster models are ongoing.

Acknowledgment. This work was supported by the NWO/ACTS hydrogen program. Z.-w.Q. thanks Prof. M. C. van Hemert for help with the Gaussian 03 program.

Supporting Information Available: Optimized Cartesian coordinates of the neutral $(TiO_2)_n$ and positively charged $(TiO_2)_n^+$ nanoclusters and a full citation of ref 42. This material is available free of charge via the Internet at http://pubs.acs.org.

References and Notes

(1) Grätzel, M. *Nature* **2001**, *414*, 338.
(2) Fujishima, A.; Honda, K. *Nature* **1972**, *238*, 37.
(3) Linsebigler, A. L.; Lu, G.; Yates, J. T., Jr. *Chem. Rev.* **1995**, *95*, 735.
(4) Diebold, U. *Surf. Sci. Rep.* **2003**, *48*, 53.
(5) Agrios, A. G.; Pichat, P. *J. Appl. Electrochem.* **2005**, *35*, 655.
(6) Hoffmann, M. R.; Martin, S. T.; Choi, W.; Bahnemann, D. *Chem. Rev.* **1995**, *95*, 69.
(7) Volodin, A. M. *Catal. Today* **2000**, *58*, 103.
(8) Thompson, T. L.; Yates, J. T., Jr. *Chem. Rev.* **2006**, *106*, 4428.
(9) Hagfeldt, A.; Grätzel, M. *Chem. Rev.* **1995**, *95*, 49.
(10) Wang, Y.; Herron, N. *J. Phys. Chem.* **1991**, *95*, 525.
(11) (a) Pascual, J.; Camassel, J.; Mathieu, H. *Phys. Rev. Lett.* **1977**, *39*, 1490. (b) Tang, H.; Berger, H.; Schmid, P. E.; Lévy, F.; Burri, G. *Solid State Commun.* **1977**, *23*, 161.
(12) Sato, S. *Chem. Phys. Lett.* **1986**, *123*, 126.
(13) Asahi, R.; Morikawa, T.; Ohwaki, T.; Aoki, K.; Taga, Y. *Science* **2001**, *293*, 269.
(14) Umebayashi, T.; Yamaki, T.; Itoh, H.; Asai, K. *Appl. Phys. Lett.* **2002**, *81*, 454.
(15) Ohno, T.; Mitsui, T.; Matsumura, M. *Chem. Lett.* **2003**, *32*, 364.
(16) Khan, S. U. M.; Al-Shahry, M.; Ingler, W. B., Jr. *Science* **2002**, *297*, 2243.
(17) Sakthivel, S.; Kisch, H. *Angew. Chem., Int. Ed.* **2003**, *42*, 4908.
(18) Nakamura, R.; Tanaka, T.; Nakato, Y. *J. Phys. Chem. B* **2004**, *108*, 10617.
(19) Stewart, S. J.; Fernández-García, M.; Belver, C.; Mun, B. S.; Requejo, F. G. *J. Phys. Chem. B* **2006**, *110*, 16482.
(20) Paulose, M.; Mor, G. K.; Varghese, O. K.; Shankar, K.; Grimes, C. A. *J. Photochem. Photobiol., A* **2006**, *178*, 8.
(21) Kuznetsov, V. N.; Serpone, N. *J. Phys. Chem. B*, in press.
(22) Boschloo, G.; Fitzmaurice, D. *J. Phys. Chem. B* **1999**, *103*, 2228.
(23) Nakato, Y.; Tsumura, A.; Tsubomura, H. *J. Phys. Chem.* **1983**, *87*, 2402.
(24) Nakamura, R.; Okamura, T.; Ohashi, N.; Imanishi, A.; Nakato, Y. *J. Am. Chem. Soc.* **2005**, *127*, 12975.
(25) Ranade, M. R.; Navrotsky, A.; Zhang, H. Z.; Banfiled, J. F.; Elder, S. H.; Zaban, A.; Borse, P. H.; Kulkarni, S. K.; Doran, G. S.; Whitfield, H. J. *Proc. Natl. Acad. Sci.* **2002**, *99* (Suppl. 2), 6476.
(26) Muscat, J.; Swamy, V.; Harrison, N. M. *Phys. Rev. B* **2002**, *65*, 224112.
(27) Zhang, H.; Banfield, J. F. *J. Mater. Chem.* **1998**, *8*, 2073.
(28) (a) Zhai, H.-J.; Wang, L.-S. *J. Am. Chem. Soc.* **2007**, *129*, 3022. (b) Wu, H.; Wang, L.-S. *J. Chem. Phys.* **1997**, *107*, 8221. (c) Yu, W.; Freas, R. B. *J. Am. Chem. Soc.* **1990**, *112*, 7126.
(29) (a) Matsuda, Y.; Bernstein, E. R. *J. Phys. Chem. A* **2005**, *109*, 314. (b) Demyk, K.; van Heijnsbergen, D.; von Helden, G.; Meijer, G. *Astron. Astrophys.* **2004**, *420*, 547. (c) Gail, H.-P.; Sedlmayr, E. *Faraday Discuss.* **1998**, *109*, 303.
(30) Qu, Z.-W.; Kroes, G.-J. *J. Phys. Chem. B* **2006**, *110*, 23306.
(31) Rossmeisl, J.; Qu, Z.-W.; Zhu, H.; Kroes, G.-J.; Nørskov, J. K. *J. Electroanal. Chem.* **2007**, *607*, 83.
(32) Howe, R. F.; Grätzel, M. *J. Phys. Chem.* **1987**, *91*, 3906.
(33) Micic, O. I.; Zhang, Y.; Cromack, K. R.; Trifunac, A. D.; Thurnauer, M. C. *J. Phys. Chem.* **1993**, *97*, 7277.
(34) Nakaoka, Y.; Nosaka, Y. *J. Photochem. Photobiol., A* **1997**, *110*, 299.
(35) Kisumi, T.; Tsujiko, A.; Murakoshi, K.; Nakato, Y. *J. Electroanal. Chem.* **2003**, *545*, 99.
(36) Bahnemann, D. W.; Hilgendorff, M.; Memming, R. *J. Phys. Chem. B* **1997**, *101*, 4265.
(37) (a) Hamad, S.; Catlow, C. R. A.; Woodley, S. M.; Lago, S.; Mejias, J. A. *J. Phys. Chem. B* **2005**, *109*, 15741. (b) Matsui, M.; Akoagi, M. *Mol. Simul.* **1991**, *6*, 239.
(38) Qu, Z.-W.; Kroes, G.-J. *J. Phys. Chem. B* **2006**, *110*, 8998.
(39) Persson, P.; Gebhardt, J. C. M.; Luneel, S. *J. Phys. Chem. B* **2003**, *107*, 3336.
(40) Lundqvist, M. J.; Nilsing, M.; Persson, P.; Lunell, S. *Int. J. Quantum Chem.* **2006**, *106*, 3214.
(41) Barnard, A. S.; Erdin, S.; Lin, Y.; Zapol, P.; Halley, J. W. *Phys. Rev. B* **2006**, *73*, 205405.
(42) Frisch, M. J.; Trucks, G. W.; Schlegel, H. B.; Scuseria, G. E.; Robb, M. A.; Cheeseman, J. R.; Montgomery, J. A., Jr.; Vreven, T.; Kudin, K. N.; Burant, J. C.; Millam, J. M.; Iyengar, S. S.; Tomasi, J.; Barone, V.; Mennucci, B.; Cossi, M.; Scalmani, G.; Rega, N.; Petersson, G. A.; Nakatsuji, H.; Hada, M.; Ehara, M.; Toyota, K.; Fukuda, R.; Hasegawa, J.; Ishida, M.; Nakajima, T.; Honda, Y.; Kitao, O.; Nakai, H.; Klene, M.; Li, X.; Knox, J. E.; Hratchian, H. P.; Cross, J. B.; Bakken, V.; Adamo, C.; Jaramillo, J.; Gomperts, R.; Stratmann, R. E.; Yazyev, O.; Austin, A. J.; Cammi, R.; Pomelli, C.; Ochterski, J. W.; Ayala, P. Y.; Morokuma, K.; Voth, G. A.; Salvador, P.; Dannenberg, J. J.; Zakrzewski, V. G.; Dapprich, S.; Daniels, A. D.; Strain, M. C.; Farkas, O.; Malick, D. K.; Rabuck, A. D.; Raghavachari, K.; Foresman, J. B.; Ortiz, J. V.; Cui, Q.; Baboul, A. G.; Clifford, S.; Cioslowski, J.; Stefanov, B. B.; Liu, G.; Liashenko, A.; Piskorz, P.; Komaromi, I.; Martin, R. L.; Fox, D. J.; Keith, T.; Al-Laham, M. A.; Peng, C. Y.; Nanayakkara, A.; Challacombe, M.; Gill, P. M. W.; Johnson, B.; Chen, W.; Wong, M. W.; Gonzalez, C.; Pople, J. A. *Gaussian 03*, revision C.02; Gaussian, Inc.: Wallingford, CT, 2004.
(43) Kohn, W.; Sham, L. J. *Phys. Rev.* **1965**, *140*, A1133.
(44) Becke, A. D. *J. Chem. Phys.* **1993**, *98*, 5648.
(45) Lee, C.; Yang, W.; Parr, R. G. *Phys. Rev. B* **1988**, *37*, 785.
(46) Dunning, T. H., Jr.; Hay, P. J. In *Modern Theoretical Chemistry*; Schaefer, H. F., III, Ed.; Plenum, New York, 1976; Vol. 3, p 1.
(47) Hay, P. J.; Wadt, W. R. *J. Chem. Phys.* **1985**, *82*, 270.
(48) Wadt, W. R.; Hay, P. J. *J. Chem. Phys.* **1985**, *82*, 284.
(49) Hay, P. J.; Wadt, W. R. *J. Chem. Phys.* **1985**, *82*, 299.
(50) Stratmann, R. E.; Scuseria, G. E.; Frisch, M. J. *J. Chem. Phys.* **1998**, *109*, 8218.
(51) Bauernschmitt, R.; Ahlrichs, R. *Chem. Phys. Lett.* **1996**, *256*, 454.
(52) Casida, M. E.; Jamorski, C.; Casida, K. C.; Salahub, D. R. *J. Chem. Phys.* **1998**, *108*, 4439.
(53) Chase, M. W., Jr. NIST-JANAF Themochemical Tables, Fourth Edition, *J. Phys. Chem. Ref. Data, Monogr.* **1998**, *No. 9*, 1−1951.
(54) NIST Chemistry WebBook, NIST Standard Reference Database Number 69, June 2005 Release. http://webbook.nist.gov/chemistry/.
(55) Cox, J. D.; Wagman, D. D.; Medvedev, V. A. *CODATA Key Values for Thermodynamics*; Hemisphere Publishing Corp.: New York, 1984; p 1.